Controlling distance, size and concentration of nanoconjugates for optimized LSPR based biosensors

Controlling distance, size and concentration of nanoconjugates for optimized LSPR based biosensors

Ankan Dutta Chowdhury[a], Fahmida Nasrin[b], Rupali Gangopadhyay[c,#], Akhilesh Babu Ganganboina[a], Kenshin Takemura[b], Ikko Kozaki[d], Hiroyuki Honda[d], Toshimi Hara[e], Fuyuki Abe[e], Sungjo Park[f], Tetsuro Suzuki[g], Enoch Y. Park[a,b,*]

[a] *Research Institute of Green Science and Technology, Shizuoka University, 836 Ohya Suruga-ku, Shizuoka 422-8529, Japan*

[b] *Department of Bioscience, Graduate School of Science and Technology, Shizuoka University, 836 Ohya Suruga-ku, Shizuoka 422-8529, Japan*

[c] *University of Engineering and Management, Action Area III, New Town, Kolkata 100156, India*

[d] *Department of Biomolecular Engineering, Graduate School of Engineering, Nagoya University, Nagoya 464-8603, Japan*

[e] *Department of Microbiology, Shizuoka Institute of Environment and Hygiene, 4-27-2, Kita-13 Ando, Aoi-ku, Shizuoka 420-8637, Japan*

[f] *Department of Cardiovascular Medicine, Mayo Clinic College of Medicine and Science, Mayo Clinic, 200 First Street SW, Rochester, MN, 55905, U.S.A.*

[g] *Department of Infectious Diseases, Hamamatsu University School of Medicine, 1-20-115 Higashi-ku, Handa-yama, Hamamatsu 431-3192, Japan*

---

[*]Corresponding author. Research Institute of Green Science and Technology, Shizuoka University, 836 Ohya Suruga-ku, Shizuoka 422-8529, Japan. E-mail: park.enoch@shizuoka.ac.jp

[#]Present Address: Sister Nivedita University, DG Block (Newtown), Action Area I, 1/2, Newtown, Kolkata 700156, India

E-mail: ankan.dutta.chowdhury@shizuoka.ac.jp (A.D. Chowdhury), fahmida.nasrin.17@shizuoka.ac.jp (F. Nasrin), camrg@iacs.res.in (R. Gangopadhyay), akhilesh.babu.ganganboina@shizuoka.ac.jp (A.B. Ganganboina), takemura.kenshin16@shizuoka.ac.jp (K. Takemura), kozaki.ikkou@b.mbox.nagoya-u.ac.jp (I. Kozaki), honda@chembio.nagoya-u.ac.jp (H. Honda), toshimi1_hara@pref.shizuoka.lg.jp (T. Hara), fuyuki1_abe@pref.shizuoka.lg.jp (F. Abe), park.sungjo@mayo.edu (SP), tesuzuki@hama-med.ac.jp (T. Suzuki), park.enoch@shizuoka.ac.jp (E.Y. Park)

Abstract

In this report, we have examined the distance- and size-dependent localized surface plasmon resonance (LSPR) between fluorescent quantum dots (QDs) and adjacent gold nanoparticles (AuNPs) to provide a comprehensive evaluation, aiming for practical application in biosensing platform. A series of peptides with different chain lengths, connected between QDs and AuNPs is initially applied to prepare various CdSe QDs-peptide-AuNP systems to optimize LSPR signal. Separation distance between two nanoparticles of these systems before and after conjugation is also confirmed by quantum mechanical modeling and corroborated with their LSPR influenced fluorescence variations. After detailed optimizations, it can be noted that larger sized AuNPs make strong quenching of QDs, which gradually shows enhancement of fluorescence with the increment of distance and the smaller sized AuNPs. Depending on the requirement, it is possible to tune the optimized structure of the CdSe QD-peptide-AuNP nanostructures for the application. In this work, two different structural designs with different peptide chain length are chosen to construct two biosensor systems, observing their fluorescence enhancement and quenching effects, respectively. Using different structural orientation of these biosensors, two nanoconjugates has applied for detection of norovirus and influenza virus, respectively to confirm their application in sensing.

Keywords: Distance dependency, Localized surface plasmon resonance (LSPR), Peptide, Tunable biosensor, Virus detection

1. Introduction

Development of biosensing devices with low detection level has become extremely important (Chowdhury et al. 2019; Dutta Chowdhury et al. 2018; Hassanpour et al. 2018; Tereshchenko et al. 2017) day by day as a significant and increasing portion of the world's population is suffered every year from viral diseases. Over the last two decades, a great deal of research has been devoted to finding suitable techniques for enhancing the sensitivity of different detection platforms in biosensing (Ahmed et al. 2014; Haes and Van Duyne 2002; Nasrin et al. 2018; Qiu et al. 2017). Among these, localized surface plasmon resonance (LSPR)-based optical biosensor has emerged considerably due to its significant application potential (Acimovic et al. 2014; Adegoke et al. 2017; Brolo 2012; Jeon et al. 2018; Satija et al. 2015; Takemura et al. 2017). To improve the performance of sensing platforms, a combination of the fluorescent quantum dots (QDs) with the plasmonic metal nanoparticles has been exploited in different manners (Adegoke et al. 2017; Ganganboina and Doong 2018; Schreiber et al. 2014; Shi et al. 2015). As a detecting signal, the fluorescence intensity of QD is highly sensitive to the concentration of target analytes as well as the shape, size of the nanoparticle, refractive index, and distance between the surface polarons of adjacent metal nanoparticles (Oh et al. 2017; Pan et al. 2016) proper adjustment which is necessary for device performance. Recently, few LSPR-based fluorometric reports have claimed to achieve the desired low-level detection limit by altering the distance between the inorganic QDs and gold nanoparticles (AuNPs) (Feizpour et al. 2015). However, the successful application of the system for point-of-care detection using clinically isolated samples is not reported there. Although the parameters for optimizing LSPR are individually examined in different applications, the system has not been appropriately explored earlier. Moreover, their reliability and reproducibility also remain questionable as the parameters are not optimized in detail. Combining all the parameters

in a single system, a generalized biosensing platform can be formed for the detection of several analytes, via careful selection of their exact and optimized conditions.

In this report, a series of Cadmium Selenium (CdSe) QD-peptide-AuNP nanoconjugate systems with different peptide linkers has been designed to understand the LSPR behavior. The designed nanoconjugates were conjugated with a terminal amine, thiol, and intermediate –COOH group for binding QDs, AuNPs, and antibodies, respectively, varying the distance between nanoduos. The influence of the separation between QD and AuNP on the output of an LSPR-based sensing has been investigated using norovirus-like particles (NoV-LP) and influenza virus. Designed peptides were exposed to the detection of NoV-LPs and the influenza virus after optimizing their structure and other parameters. The efficiency of the system, using complex matrices like clinically isolated samples, has proved the system to be a potential platform for virus detection using multiple detection principles. These systems apply to the ultra-sensitive detection of small biomolecules like viruses, bacteria, proteins, etc. in a wide detection range, which is in the utmost requirement for point of care diagnosis.

2. Materials and methods

2.1. Chemicals and synthesis of peptides, antigen, and antibody

All chemical lists including antibody and virus information are given in the Supplementary material.

2.2 Preparation of water-soluble CdSe QDs

CdSe QDs were prepared according to the widely used standard protocol (Yu et al. 2003). To make the QDs in an aqueous medium, ligand exchange reaction was carried out with mercaptoacetic acid according to our previous work (Huang et al. 2007).

2.3 Seed preparation, synthesis, and growth of AuNPs:

In this report, gold nanoparticles with six different sizes (15, 25, 35, 45, 60, and 80 nm) were synthesized, and their effect on fluorescence intensity of CdSe QDs was investigated. Initially, a seed solution of AuNPs was synthesized by reducing 100 mL of 1 mM $HAuCl_4$ at pH 6.2–6.5 by dissolving 10 mL of 38.8 mM Na_3Ctr at100°C (Leng et al. 2015). A variable volume of seed solution was added with 227 µL of 44.7 mM $HAuCl_4 \cdot 3H_2O$ to synthesize the AuNPs growth solution. Finally, 176 µL of 38.8 mM $Na_3Ctr \cdot 2H_2O$ was added with continuous stirring until the color of the solution changes from colorless to wine red (Leng et al. 2015).

2.4 Preparation of the sensing probe

We have designed six peptides containing thiol group in one end and amine group in another end (listed in **Fig. S1**), which was covalently conjugated with the free carboxylic group of mercaptopropionic acid (MPA)-capped CdSe QDs by EDC/NHS chemistry eventually (Adegoke et al. 2016b). Then, AuNPs were conjugated to the end via the thiol group to prepare the QD-peptide-AuNP nanocomposite (**Scheme of Fig. 5a**). For all conjugation process between QDs and AuNPs, the concentration ratio always maintained at 2:1 as the particle size of QD is small even compared to the smallest size of AuNP used in this study. The particle numbers of these nanoparticles are calculated in 10^9 particle mL^{-1}, by the UV spectra dependent Lambert-Beers law. The mixture was stirred at 7°C for 2–3 h to synthesize the sensing probe, where the AuNPs and QDs were linked by the antibody-conjugated peptide. Before peptide linkage, EDC/NHS reaction was performed to link the anti-NoV antibody covalently with the free carboxyl group of peptides. For the antibody binding, each of the peptides contains two carboxylic acid groups of aspartic acid (D) on its structure (**Fig. S1**). After completing the conjugation, the solution was purified by centrifuging for 5 min at 3000 × g and dissolved in 2 mL of ultrapure water.

2.5 Quantum mechanical modeling

Simulation regarding the interaction between CdSe QDs and AuNPs in CdSe QD-peptide-AuNP nanocomposites has been calculated using density functional theory (DFT) as implemented in the Gaussian 03 (Frisch et al. 2009) suite of program and given in Supplementary Material.

2.6. Physicochemical analysis and fluorometric detection of viruses using QD-peptide-AuNP sensing probe

All analytical methods, including fluorometric detection of virus-like particles are given in the Supplementary material.

3. Results and Discussion

3.1. Characterizations of AuNPs and CdSe QDs

By inoculating the various amounts of Au^{3+} solution with as-synthesized gold seeds, the AuNPs with sizes escalating from 20 to 80 nm were produced. **Fig. 1a–f** shows the typical transmission electron microscopy (TEM) images of the different AuNPs synthesized using the pH-controlled synthetic protocol. In the case of the seed solution in **Fig. 1a**, the nanoparticles are highly monodispersed in nature with an average diameter of 15.4 ± 0.5 nm. To achieve the bigger particle size with improved homogeneity, the growth reactions were initiated simply by adding larger seed nanoparticles to the premixed solutions of Au^{3+} and sodium citrate. As shown in the TEM images of **Fig. 1b–f**, the produced AuNPs are in increasing sizes of 21, 32, 41, 65, and 80 nm, where most of the nanoparticles are in quasi-spherical shape. It is noteworthy that the calculated sizes are relatively close to their expected sizes of 25, 35, 45, 60, and 80 nm. There are very few numbers of triangular nanocrystal formed only in the case

of particles above 60 nm. Ignoring the presence of these insignificant numbers of non-spherical particles, the average diameters of the AuNPs are determined and tabulated in the Table (**Fig. 1i**). We have also measured the average particle diameters of AuNP using Haiss' equation (with B1 = 3.00 and B2 = 2.20) based on the UV-vis spectra of the AuNP seeds (**Fig. 1g**) (Haiss et al. 2007). Smaller AuNPs primarily absorb the wavelength around 525 nm. With increasing the size, the absorption maxima are gradually shifted towards longer wavelengths with a significant increase in scattering. Larger spheres scatter more due to the larger optical cross-sections. Their albedo (a ratio of scattering to total extinction) increases with size, clearly indicating the successful growth of the nanoparticles. In addition, their hydrodynamic size distributions were further calculated from the dynamic light scattering (DLS) measurement (**Fig. 1h**), which also corroborated the results obtained from TEM images. The zeta potential of synthesized AuNPs also follows the expected trends of surface charges increasing along with an increase in particle sizes. The TEM image, along with size distribution, has presented in **Fig. S2.**

3.2. Effect of AuNPs size and peptide length on the fluorescence of CdSe QD-peptide-AuNP nanoconjugate

The enhancement or quenching effect of AuNPs size and peptide length on fluorescence intensities of CdSe QD-peptide-AuNP nanoconjugate is investigated. The absorption spectra of different AuNPs display the first exciton transition peaks at 535 nm, whereas the fluorescence spectrum of CdSe QDs shows a Gaussian-shaped peak located at 638 nm (**Fig. S3**). Six different-sized AuNPs (15, 25, 35, 45, 60, and 80 nm) were linked with CdSe QDs using six different lengths of peptide linkers. Therefore, a total number of thirty-six possible combinations of CdSe QD-peptide-AuNP nanoconjugates are obtained, and their fluorescence

176 intensities originating from CdSe QD was measured in PBS buffer at pH 6.7 (**Fig. 2a–f)**.
177 Increasing the size of the conjugated AuNPs increased the fluorescence quenching regardless
178 of the peptide length. In the case of 80 nm AuNP (**Fig. 2a**), the fluorescence of CdSe QDs has
179 been completely quenched for all the nanoconjugates irrespective of the peptide length. On the
180 other hand, with 15 nm AuNPs (**Fig. 2f**), the fluorescence of QDs is enhanced gradually as the
181 distance between the QDs and AuNP increased from 3 nm to 18 nm, regulated by the peptide
182 length. If QDs and AuNP are separated by a distance of 1.8 nm (6 amino acid peptide length),
183 quenching occurred irrespective of AuNP size, while the degree of the quenching becomes
184 stronger as the AuNP size increases (**Fig. 2a**). The smaller sized AuNPs have negligible LSPR
185 absorption and hence quench the fluorescence emission of the QDs less effectively, following
186 the nanometal surface energy transfer mechanism (Yun et al. 2005). Also, the local field
187 enhancement effect of the AuNPs can enhance fluorescence emission significantly (Feng et al.
188 2015). However, with larger AuNPs, strong LSPR absorption bands can overlap with the
189 emission band of the QDs. The energy transfer efficiency depends on the separation between
190 the nanoconjugates, dominated by the dipole-dipole interaction (Zhang et al. 2014). Therefore,
191 80 nm AuNP displays the highest quenching efficiency due to the increased spectral overlap
192 of the LSPR band with the emission band of CdSe QDs.

193 As shown in **Fig. 2a–f**, in all the nanoconjugates with QDs and AuNP separated by a
194 distance of only 1.8 nm (shortest separated distance), exhibit quenching behavior irrespective
195 of AuNP sizes. However, the quenching effect is transformed into enhancement when the
196 distance between the nanoduo (QDs and AuNP) increases from 1.8 to 15.5 nm (from 6 to 18
197 amino acid peptides). The quantum efficiency and the emission intensity of the CdSe QDs can
198 be either enhanced or quenched by the equilibrium of two ways of the electron transfer process
199 of non-radiative energy transfer (NRET) and local field enhancement effect (LFEE) (Feng et
200 al. 2015; Zhang et al. 2014). When the nanoduo is close enough, NRET dominates, resulting

in the fluorescence quenching. With the increase in the distance among the nanoduo, the LFEE becomes predominating over the NRET, contributing to the enhancement of fluorescence intensity. The emission intensity reaches the maximum at an optimal distance of about 16 nm between the particles.

3.3. Studies on bare CdSe nanostructure to build up the initial structures of peptide-CdSe QDs assembly

The goal of any simulation is to predict or analyze the real systems' properties that are not directly observable. From the quantum mechanical analysis revealed that the distance between the terminals with the bare peptide CDDK (in folded condition) was found to be around 0.4 nm, increased to 0.7 nm after linking with CdSe (~0.5–0.6 nm) in one side, and further enhanced to 0.97 nm after AuNP (0.5 nm) attachment to complete the nanoduo particle structure. Although for the sake of easy simulation, both the nanoparticles are taken in a much smaller size than their original sizes (5 nm, 35 nm), these results can qualitatively represent the behavior of the real system.

The $(CdSe)_6$ has been chosen as it is the smallest 3D cluster (D_{3d}) leading to spherical CdSe nanoparticles and retains the basic structure of $(CdSe)_N$ when $N \geq 7$. We have initially stabilized the structure of $(CdSe)_6$ with MPA. Here both O and S atoms are linked with Cd atoms, and an eight-member ring-like structure is evolved with an S-Cd distance of 0.27 nm. This structure is unaffected when connected with a small peptide chain of X_1 (**Fig. S4a–c**), with an S-Cd distance shorter than 0.2 nm. The eight-member ring is almost retained even after AuNP is linked with the peptide-CdSe assembly when the length of the S-Cd bond is reduced by ~0.1 nm (0.26 nm). This result is in pace with the earlier finding, indicating stronger bonding of CdSe QD with the peptide chain even after the linkage of AuNP (Cui et al. 2015). With the

225 increase in peptide chain length, the mode of CdSe QD linkage remains unchanged (via Cd
226 atoms), and the Cd-S distance also remains almost the same (0.25 nm) while the eight-member
227 ring is restructured to a pseudo-12-member ring (**Fig. S4**). Therefore, the attachment of CdSe
228 with peptide is quite strong that remains unaffected by the chain length as well as the folding
229 of the peptide chain. However, the peptide chain affects the ultimate structure of the
230 nanoassembly and the end-to-end separation of the nanoconjugates that are reflected in the
231 respective LSPR signal, as presented in **Fig. 3a–c**. The smallest free peptide of CDDK (X_1;
232 **Fig. S1**) with a cumulative length of 1.8 nm, produces a folded structure in **Fig. 3a** where the
233 end-to-end distance is calculated to be only 0.4 nm. By the successive addition of the CdSe and
234 the smallest unit of AuNP, the distance increases up to 0.7 and 0.97 nm, respectively.

235 It should be noted that the simulated structures of the CdSe and the AuNP are shown
236 here refer to the smallest possible clusters of those two. Looking at the increasing trend shown
237 in **Fig. 3b** and **c**, it can be expected that the simulated distance between the CdSe and the AuNP
238 becomes closer to the cumulative distance as calculated by the peptide length.

239 The fourth peptide of CGGGGGDGGGGDGGGGGK (X_4; **Fig S1)**, we have added the
240 bigger cluster of AuNP (Au_8). After the attachment of the CdSe QD and AuNP, the end-to-end
241 separation increased to 7.4 nm, which is quite close to the speculated distance of 8.5 nm, as
242 shown in **Fig. 3d**. The fluorescence enhancement of the CdSe QD, as shown in **Fig. 3e** also
243 supports the prediction parallel to the simulated structures. After attachment of the AuNP on
244 the CdSe QD-peptide assembly, the significant increase of the fluorescence indicates large
245 enough separation of these two nanoparticles, resulting in the development of the successive
246 LSPR. For the sensing application, we need to choose some optimized conditions. The system
247 has some flexibility to change its electron transfer process in response to very few analytes;
248 this is more favorable with open structure compared to the ring-like one. Keeping this in mind,
249 the peptide X_4, harboring an open structure and 7.4 nm end-to-end separation after LSPR

conjugation, offers the best possibility to switch over from enhancement to quenching behavior. This theoretical prediction will be validated through experimental results in successive sections.

3.4. Effect of AuNP concentration on the LSPR of CdSe QD-peptide-AuNP nanoconjugate

The concentration effects of CdSe QD-peptide-AuNP nanoconjugate on LSPR have been investigated in different concentrations of AuNPs, where the AuNP size is fixed at 35 nm, which is optimized in **Fig. 2d**. As shown in **Fig. 2g** in identical condition, 10^{12} AuNPs mL^{-1} had a stronger quenching effect than 10^{9} AuNPs mL^{-1}, whereas the diluted solution shows better enhancement. This can be explained by the possibility of the nonspecific interaction that increases in the closeness of the AuNPs in concentrated solutions. In the case of the excess number of AuNP present in the medium, the possibility of the nonspecific surface adsorption of QDs on the surface of AuNP increases significantly, resulting in the predominant quenching effect. However, to get the optimum condition balancing the enhancement and quenching, the concentration of 10^{9} AuNPs mL^{-1} should be optimal one (**Fig. 2g**), and this optimized AuNP concentration was used for further analysis.

3.5. Characterizations of CdSe QD-peptide X_4-AuNP nanoconjugate

Despite the clear indication of fluorescence enhancement or quenching after the successful conjugation of the CdSe QD-peptide-AuNP nanoconjugate, the composites were further characterized by some physicochemical tools viz. high-resolution TEM (HRTEM). In **Fig. 4a**, the small QDs (~5 nm) and the AuNPs (~35 nm) were closely oriented due to the covalent bonding and internal hydrogen bonding controlled by the peptide linkage. HRTEM image of an isolated nanocomposite deciphered the crystal fringes of the AuNP and the QDs,

273 situated at the adjacent position (**Fig. 4b**). In the case of elemental mapping in STEM, a cluster
274 of CdSe QD-peptideX_4-AuNP nanoconjugates has been isolated (**Fig. 4c**), in which the
275 individual elements have been observed distinctly. The nanocomposite was mapped with Au
276 and Cd (**Fig. 4d–e**), respectively, which revealed the successful linkage of CdSe QDs and
277 AuNPs through the peptide linkage. Due to the small size and low molecular weight, the
278 peptide chain was not accurately mapped. The AFM images of the nanocomposites have
279 revealed similar observations, as mentioned in **Fig. S5**, where the AuNP and CdSe QDs are
280 closely located in small separation, indicate the peptide linker's presence.

281 FTIR analysis was further carried out to reveal the involvement of the peptide in the
282 CdSe QDs, as shown in **Fig. 4f**. In the case of the bare CdSe QDs, the spectrum appeared with
283 all of its standard-transmitted peaks, particularly at 1541 cm^{-1} assigned to the asymmetric
284 carboxylate (–COO–) group (Adegoke et al. 2016a). It is noteworthy that the spectrum remains
285 almost unchanged after linking with the peptide, where some additional peaks have appeared
286 due to the conjugation. The bands observed at 3410.1 cm^{-1}, 2903.3 cm^{-1}, and 1715.6 cm^{-1}, are
287 recognized as –OH/NH_2 stretching, C–H stretching, and C–O stretching of carboxylic acid
288 respectively (Tetsuka et al. 2016). The band at 1181.1 cm^{-1} represents the twisting mode of
289 NH_3^+, which is quite common for amino acids, indicating the presence of a peptide chain
290 (Ahmed et al. 2013).

291 The nanocomposites formation was further verified by hydrodynamic diameter
292 measurement, where the CdSe QD-peptide-AuNPs nanocomposites, along with its components,
293 were determined by DLS (**Fig. 4g**). The bare CdSe QDs and AuNPs show the hydrodynamic
294 size of 5 ± 0.5 nm and 28.4 ± 1.5 nm, respectively, which almost matches that obtained during
295 their initial characterizations. In the case of CdSe QD-peptide-AuNPs nanoconjugate, it shows
296 at a diameter of 87 ± 1.5 nm, which is larger than their sizes, confirming the agglomeration. In
297 the case of the smallest (X_1) and largest (X_4) peptides in the series, the hydrodynamic radius

does not show significant changes (**Fig. S6**). But their high PDI values indicate the heterogeneous nature due to the agglomeration. The conjugation of the peptide on the CdSe QDs is also confirmed by the XPS spectra, as depicted in **Fig. 4h**. The deconvoluted C1s peak intensity has increased significantly after the addition of the peptide in the CdSe QDs. In addition, the successful conjugation of the AuNP with the CdSe QDs has also confirmed by the deconvoluted Au4f XPS spectra, as depicted in **Fig. 4i**. The Au4f peak has appeared in the spectrum of CdSe QD-peptide-AuNPs nanoconjugate, which was absent for bare CdSe QD-peptide.

3.6. Application of the optimized nanoconjugate in virus sensing

Among the fluorescence results from all the thirty-six optimized nanostructures, two CdSe QD-peptide-AuNP nanostructures with the peptide length of 7.4 nm (X_4) and 0.3 nm (X_1, **Fig. S1**) have been chosen for virus detection, employing their fluorescence enhancement and quenching effect. Before proceeding to virus detection, the control experiments of the virus particles with bare CdSe QDs, AuNPs, and CdSe QDs-peptide-AuNP without antibody conjugation were carried out to confirm any nonspecific binding (**Fig. S7**). 100 ng mL^{-1} virus solution is physically mixed with 10^9 particles mL^{-1} of bare AuNP and CdSe QDs. The surface of AuNP adsorbed some virus particles; however, it is not significantly high to interrupt the sensing experiments. As the virus surfaces are negatively charged, it is unlikely to adsorbed on the negatively charged AuNP or CdSe QD and specifically interact with the free antibodies attached on the peptides (**Fig S7a**). The same phenomenon has also observed in the fluorescence spectra of CdSe-peptide-AuNP without antibody conjugation, eliminating the non-specific interaction of the virus (**Fig S7b**). Then the CdSe QD-peptideX_4-AuNP nanocomposite has been used to detect NoV-LPs (30–40 nm), creating steric hindrance on the

path of LSPR between CdSe QDs and AuNPs (the TEM image of NoV-LP is provided in **Fig. S8**). Alternatively, quenched fluorescent CdSe QD-peptideX_1-AuNP nanocomposite has been applied to detect a relatively larger sized influenza virus (100 – 150 nm), recovering the fluorescence by obstructing the electron transfer.

3.6.1. Fluorescence quenching of CdSe QD-peptideX_4-AuNP nanoconjugates

The CdSe QD-peptideX_4-AuNP nanoconjugate shows the apparent enhancement of fluorescence compared to the bare CdSe QDs due to the LSPR-induced effect (**Fig. 5a)**. According to our hypothesis, in the present of the virus in the system, the antibodies can specifically bind to the virus. As the antibodies are situated in the transposition to each other, it can be anticipated that the bound viruses can produce enough steric repulsion to hamper the LSPR between the AuNPs and CdSe QDs (Nasrin et al. 2018). As a result, the fluorescence intensities have been gradually decreased with the increasing concentration of the NoV-LPs (**Fig. 5b**). The ratio of change in fluorescence intensities (gradually quenching) to initial fluorescence ($\Delta F/F_i$) is plotted against the virus concentration in **Fig. 5c**. Excellent linearity was observed with the increase of the NoV-LP concentration from 0.1 pg to 50 ng mL^{-1} beyond which it reaches saturation. The linearity in the concentration range of 1 pg to 100 pg mL^{-1} has emphasized the calibration curve' inset. The limit of detection (LOD) is found to be 124 fg mL^{-1}, based on $3\sigma/S$ (σ is the standard deviation of the lowest signal, and S is the slope of the linear line) (Nasrin et al. 2018). Based on these results, we expect that the proposed system and the method can be an excellent alternative to the general biomolecular detection by changing the entrapped antibody and its corresponding analytes.

To verify any nonspecific interaction or interferences from any component of the sensor, the detection of the target virus was compared with other viruses and possible interfering agents.

The sensitivity of the CdSe QD-peptideX_4-AuNP nanocomposite is solely dependent on the antibody sites and for most of the common interferants matrix effects are almost negligible (**Fig. S9**). In the case of other viruses like Zika, influenza, and hepatitis E virus-like particle (HEV-LP) in the same concentration of 10 pg mL^{-1}, the sensor shows an almost negligible response, indicating the designed LSPR-based biosensor was highly specific for the targeted NoV-LP.

The ultimate goal of biosensors is to detect any viral infection based on its RNA measurement ability. To evaluate the applicability in clinical samples, the developed sensor was further exposed to the detection of inactivated clinical NoV. RNA copy number in the concentration range from 10^2 to 10^5 RNA copies mL^{-1} has been measured by the CdSe QDs-peptideX_4-AuNP sensor and plotted in terms of fluorescence (**Fig. S10a**). Satisfactory linearity of R^2 = 0.985 was maintained in the calibration curve (**Fig. S10b**). The LOD has been calculated as 113 RNA copies mL^{-1} from the same equation, as mentioned above. The linearity and low LOD prove the sensor system's ability to detect the real virus.

3.6.2. Recovering of fluorescence intensity of CdSe QD-peptideX_1-AuNP nanoconjugates

In the CdSe QD-peptideX_1-AuNP, a completely reverse methodology has been examined to detect the influenza virus. In contrast to the previous system, the addition of the virus to bind the antibodies should restrict the process of the LSPR between the AuNPs and CdSe QDs. To this end, the quenching effect from the AuNP is expected to be gradually lowered with the increasing concentration of the influenza virus. The results of the LSPR-induced immunofluorescence enhancement for the detection of the influenza virus (**Fig. 5d**). The corresponding linear calibration curve (**Fig. 5e**) where the LOD is found of 14.6 fg mL^{-1}, based on $3\sigma/S$.

3.7 Spiked NoV-LP detection in serum by CdSe QD-peptideX$_4$-AuNP nanoconjugates

To understand the sensing capability in real sample analysis, the CdSe QD-peptideX$_4$-AuNP nanoconjugates have applied to a series of six samples with increasing concentrations of spiked NoV-LP in 10% serum solution followed by the calculation of the recovery using the method. As shown in **Table 1**, the recovery of 106 ± 2.5% was observed when a low concentration of 10^{-12} g mL^{-1} was spiked. 96 – 106% recovery was found when the concentration range of $10^{-12} – 5 \times 10^{-10}$ g mL^{-1} of NoV-LPs was spiked into the serum solution. Although the matrix affects the sensor a little, which is obvious in the case of peptide and AuNP containing system, however, the relative standard deviations for all the spiking analyses are in the range of 1.4 – 3.7 % (n = 3), clearly indicating the sensing system's ability for analytical performance.

Conclusion

In this work, based on the physical significance of LSPR, we established a tunable and versatile sensing system using CdSe QD-peptide-AuNP nanoconjugate for ultrasensitive biosensing. For the detailed investigation, several CdSe QD-peptide-AuNP nanoconjugates were designed by varying the length of the peptide chain used as linker, size, and concentration of AuNPs, and the resulting changes in fluorescence intensities were examined. Theoretical simulation is performed to validate the experimental separation distance between the terminal nanoduos. The close interaction of CdSe QDs and AuNP shows a strong quenching effect of QDs fluorescence, which gradually shows enhancement of fluorescence with the increment of distance. Depending on the outcome of spectroscopic studies, two systems were chosen for the

393 application and successfully applied for the sensing of NoV and influenza virus, respectively,
394 using two different sized peptides, following exactly opposite sensing mechanism. In both
395 cases, excellent linearity was observed with virus concentration with LODs of 124 fg mL^{-1} for
396 NoV-LP and 14.6 fg mL^{-1} for the Influenza virus. In this emerging field of LSPR-based
397 biosensing, we hope that the thorough investigation of this present study can give a useful
398 direction in the future.

399

400 Acknowledgments

401 Authors thanks to Professor K. Morita of Institute of Tropical Medicine Nagasaki
402 University and Dr. Tian-Cheng Li of National Institute of Infectious Diseases for providing the
403 Zika virus and hepatitis E virus-like particle (HEV-LP), respectively. A.D.C. and A.B.G.
404 sincerely thank the Japan Society for the Promotion of Science (JSPS) for a postdoctoral
405 fellowship (Grant Nos. 17F17359 and 19F19064). R.G. acknowledges BRAF, Pune (India),
406 for providing computational facilities.

407 Competing interests

408 The authors declare no competing interests.

409 Appendix A. Supplementary Materials

410 Supplementary materials associated with this article can be found in the online
411 version at.

412

413 References

414 Acimovic, S.S., Ortega, M.A., Sanz, V., Berthelot, J., Garcia-Cordero, J.L., Renger, J., Maerkl,
415 S.J., Kreuzer, M.P., Quidant, R., 2014. Nano Lett. 14(5), 2636–2641.
416 Adegoke, O., Morita, M., Kato, T., Ito, M., Suzuki, T., Park, E.Y., 2017. Biosen. Bioelectrons.
417 94, 513–522.
418 Adegoke, O., Nyokong, T., Forbes, P.B., 2016a. Luminescence 31(3), 694–703.
419 Adegoke, O., Seo, M.-W., Kato, T., Kawahito, S., Park, E.Y., 2016b. Biosen. Bioelectrons. 86,
420 135–142.
421 Ahmed, M.H., Byrne, J.A., McLaughlin, J., Elhissi, A., Ahmed, W., 2013. Appl. Surf. Sci. 273,
422 507–514.
423 Ahmed, S.R., Hossain, M.A., Park, J.Y., Kim, S.-H., Lee, D., Suzuki, T., Lee, J., Park, E.Y.,
424 2014. Biosen. Bioelectrons. 58, 33–39.
425 Brolo, A.G., 2012. Nat. Photonics 6(11), 709.
426 Chowdhury, A.D., Takemura, K., Li, T.-C., Suzuki, T., Park, E.Y., 2019. Nature Commun.
427 10(1), 3737.
428 Cui, Y., Lou, Z., Wang, X., Yu, S., Yang, M., 2015. Phys Chem Chem Phys 17(14), 9222–
429 9230.
430 Dutta Chowdhury, A., Ganganboina, A.B., Nasrin, F., Takemura, K., Doong, R.-a., Utomo,
431 D.I.S., Lee, J., Khoris, I.M., Park, E.Y., 2018. Anal Chem 90(21), 12464–12474.
432 Feizpour, A., Yu, X., Akiyama, H., Miller, C.M., Edmans, E., Gummuluru, S., Reinhard, B.M.,
433 2015. Small 11(13), 1592–1602.
434 Feng, A.L., You, M.L., Tian, L., Singamaneni, S., Liu, M., Duan, Z., Lu, T.J., Xu, F., Lin, M.,
435 2015. Sci Rep 5, 7779.
436 Frisch, M., Trucks, G., Schlegel, H., Scuseria, G., Robb, M., Cheeseman, J., Scalmani, G.,
437 Barone, V., Mennucci, B., Petersson, G., 2009. Wallingford, CT 32, 5648–5652.
438 Ganganboina, A.B., Doong, R.-a., 2018. Sens Actuators B 273, 1179–1186.

439 Haes, A.J., Van Duyne, R.P., 2002. J Am Chem Soc 124(35), 10596–10604.

440 Haiss, W., Thanh, N.T., Aveyard, J., Fernig, D.G., 2007. Anal Chem 79(11), 4215–4221.

441 Hassanpour, S., Baradaran, B., de la Guardia, M., Baghbanzadeh, A., Mosafer, J., Hejazi, M.,
442 Mokhtarzadeh, A., Hasanzadeh, M., 2018. Microchim. Acta 185(12), 568.

443 Huang, C.-P., Li, Y.-K., Chen, T.-M., 2007. Biosen. Bioelectrons. 22(8), 1835–1838.

444 Jeon, J., Uthaman, S., Lee, J., Hwang, H., Kim, G., Yoo, P.J., Hammock, B.D., Kim, C.S., Park,
445 Y.-S., Park, I.-K., 2018. Sens Actuators B 266, 710–716.

446 Leng, W., Pati, P., Vikesland, P.J., 2015. Environmental Science: Nano 2(5), 440–453.

447 Nasrin, F., Chowdhury, A.D., Takemura, K., Lee, J., Adegoke, O., Deo, V.K., Abe, F., Suzuki,
448 T., Park, E.Y., 2018. Biosen. Bioelectrons. 122, 16–24.

449 Oh, S.Y., Heo, N.S., Shukla, S., Cho, H.-J., Vilian, A.E., Kim, J., Lee, S.Y., Han, Y.-K., Yoo,
450 S.M., Huh, Y.S., 2017. Sci Rep 7(1), 10130.

451 Pan, M., Liang, Z., Wang, Y., Chen, Y., 2016. Sci Rep 6, 29984.

452 Qiu, S., Zhao, F., Zenasni, O., Li, J., Shih, W.-C., 2017. Nanoscale Horiz 2(4), 217–224.

453 Satija, J., Tharion, J., Mukherji, S., 2015. RSC Adv. 5(86), 69970–69979.

454 Schreiber, R., Do, J., Roller, E.-M., Zhang, T., Schüller, V.J., Nickels, P.C., Feldmann, J., Liedl,
455 T., 2014. Nat. Nanotechnol. 9(1), 74.

456 Shi, J., Chan, C., Pang, Y., Ye, W., Tian, F., Lyu, J., Zhang, Y., Yang, M., 2015. Biosen.
457 Bioelectrons. 67, 595–600.

458 Takemura, K., Adegoke, O., Takahashi, N., Kato, T., Li, T.-C., Kitamoto, N., Tanaka, T.,
459 Suzuki, T., Park, E.Y., 2017. Biosen. Bioelectrons. 89, 998–1005.

460 Tereshchenko, A., Fedorenko, V., Smyntyna, V., Konup, I., Konup, A., Eriksson, M.,
461 Yakimova, R., Ramanavicius, A., Balme, S., Bechelany, M., 2017. Biosen. Bioelectrons.
462 92, 763–769.

463 Tetsuka, H., Nagoya, A., Fukusumi, T., Matsui, T., 2016. Adv. Mat. 28(23), 4632–4638.

Yu, W.W., Qu, L., Guo, W., Peng, X., 2003. Chemistry of Materials 15(14), 2854–2860.

Yun, C., Javier, A., Jennings, T., Fisher, M., Hira, S., Peterson, S., Hopkins, B., Reich, N., Strouse, G., 2005. J Am Chem Soc 127(9), 3115–3119.

Zhang, L., Song, Y., Fujita, T., Zhang, Y., Chen, M., Wang, T.H., 2014. Adv. Mat. 26(8), 1289–1294.

470 **Graphical Abstract**

471

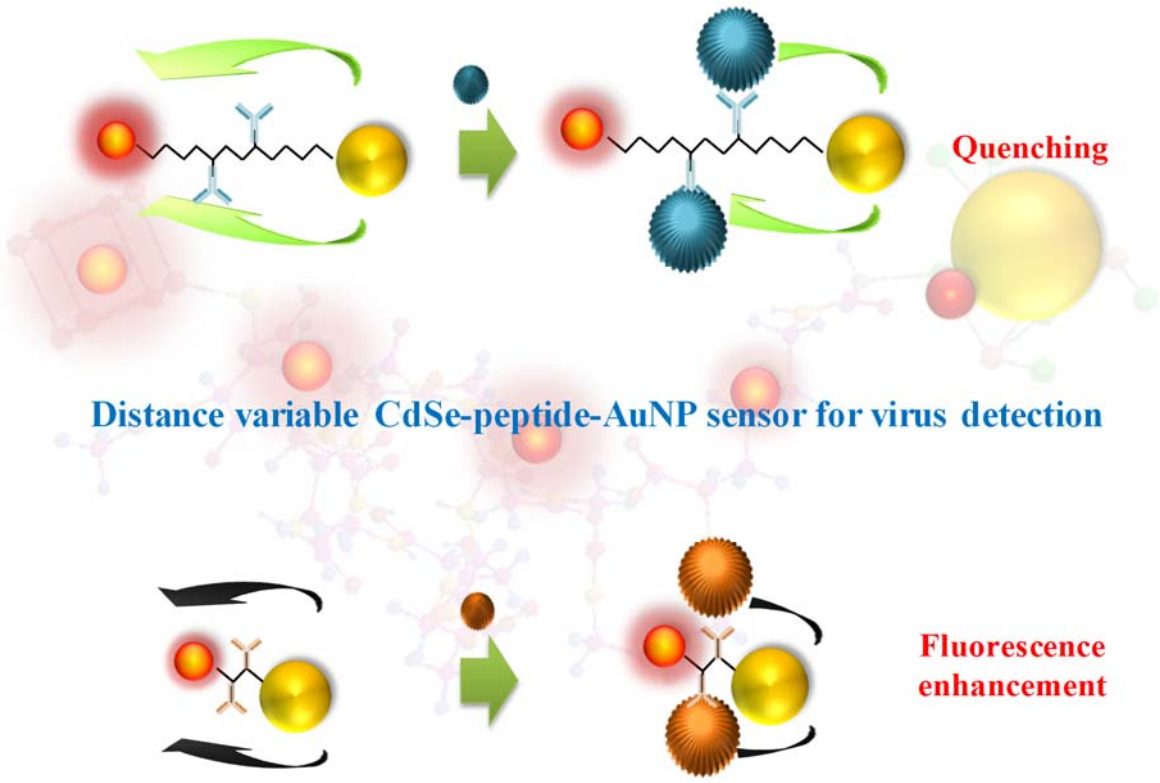

472

473

474 **Figure captions**

475 **Fig. 1.** Characterizations of different sized AuNPs. TEM images of (**a–f**) 15, 25, 35, 45, 60,
476 and 80 nm AuNP with their corresponding daylight images and size distributions, (**g**) UV-Vis
477 spectra and (**h**) DLS measurements of as-synthesized AuNPs, and (**i**) zeta potential values and
478 comparative size variation of AuNPs obtained from TEM, UV-Vis, and DLS measurements.

479 **Fig. 2.** Fluorescence spectral bar diagram of CdSe QDs in various CdSe QD-peptide-AuNP
480 nanoconjugates. Six different sizes of AuNPs at 80 nm (**a**), 60 (**b**), 45 (**c**), 35 (**d**), 25 (**e**), and
481 15 nm (**f**) combined with six different peptide length produced various fluorescence intensity
482 changes. (**g**) Effect of AuNPs concentration of 10^{12}, 10^{9}, and10^{6} mL^{-1} on the nanoconjugates
483 where all other parameters are constant.

484 **Fig. 3.** End to end distance calculation of the smallest peptide of CDDK (X_1), (**a–c**) stepwise
485 conjugation with CdSe QD and AuNP, (**d**) simulated structure of CdSe QD-peptide X_4-AuNP,
486 and (**e**) fluorescence spectra of the CdSe QDs and its LSPR effect after the formation of CdSe
487 QD-peptide X_4-AuNP nanocomposite.

488 **Fig. 4.** Characterizations of CdSe QD-peptide-AuNP nanoconjugate: (**a**) TEM image (**b**)
489 HRTEM image of CdSe QD-peptide-AuNP, showing their own fringes, (**c–e**) STEM mapping
490 of CdSe QD-peptide-AuNP with Cd and Au, (**f**) FTIR spectra (**g**) DLS hydrodynamic
491 distribution (**h**) XPS deconvoluted C1s spectra, and (**i**) XPS deconvoluted Au4f spectra.

492 **Fig. 5.** Virus detection with the sensor probe varying the peptide length: (**a**) schematic
493 illustration for the virus sensing using CdSe QD-peptide-AuNP system for two modes of
494 detection, (**b**) fluorescence emission spectra, and (**c**) corresponding calibration curve for
495 detection of 10^{-13} – 5×10^{-7} g mL^{-1} NoV-LP, (**d**) fluorescence emission spectra, and (**e**)
496 corresponding calibration curves for the detection of 10^{-14} – 10^{-10} g mL^{-1} influenza viruses.

The red circle in the calibration graphs indicates the blank point. Error bars denote the standard deviation of 3 replicate measurements.

500

501 **Table 1.** Recovery of NoV-LP in 10% serum samples (n = 3) by CdSe QD-peptideX_4-AuNP

502 sensing system.

Sample	Spike concentration (g mL^{-1})	Detected concentration (g mL^{-1})	Recovery ± R.S.D. (%)
Sensor	0	-	-
NoV-LPs	10^{-12}	1.06×10^{-12}	106 ± 2.5
	5×10^{-12}	5.2×10^{-12}	104 ± 1.5
	10^{-11}	9.6×10^{-12}	96 ± 1.5
	5×10^{-11}	5.1×10^{-11}	102 ± 2.3
	10^{-10}	9.7×10^{-11}	97 ± 1.4
	5×10^{-10}	5.3×10^{-10}	106 ± 3.7

503

Fig. 1.

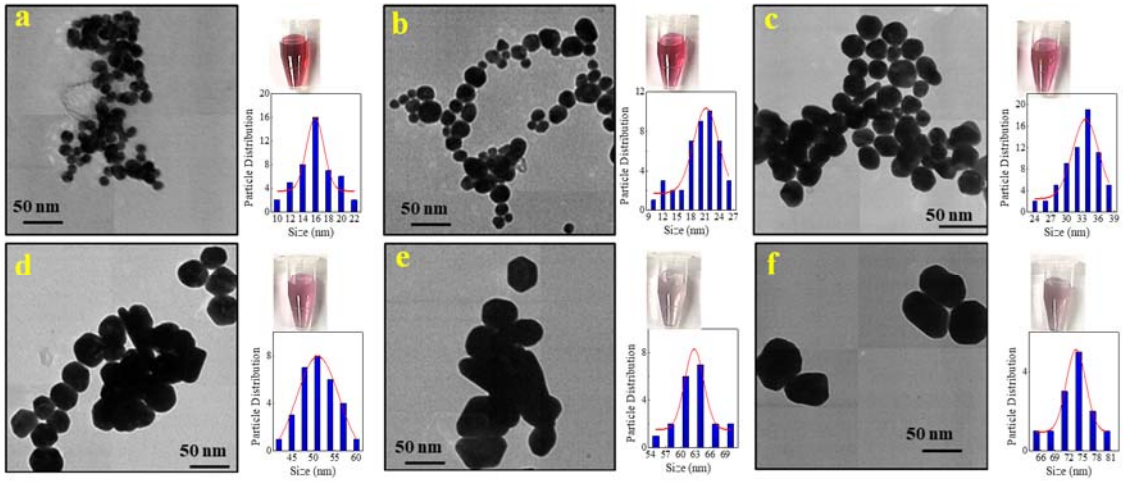

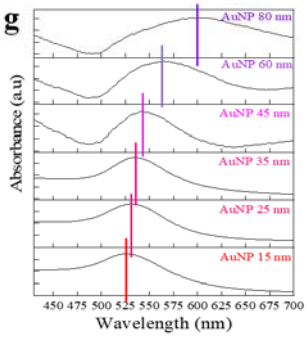

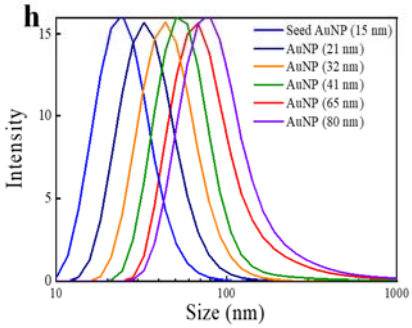

i

AuNP	Expected size	Size from DLS	Size from TEM	Zeta potential (mV)
1 (seed)	15	15	15.6	-53
2	25	21	22.5	-32
3	35	32	34.5	-26
4	45	41	50.5	-12
5	60	65	62.3	-11
6	80	80	75.2	-14

507 **Fig. 2.**

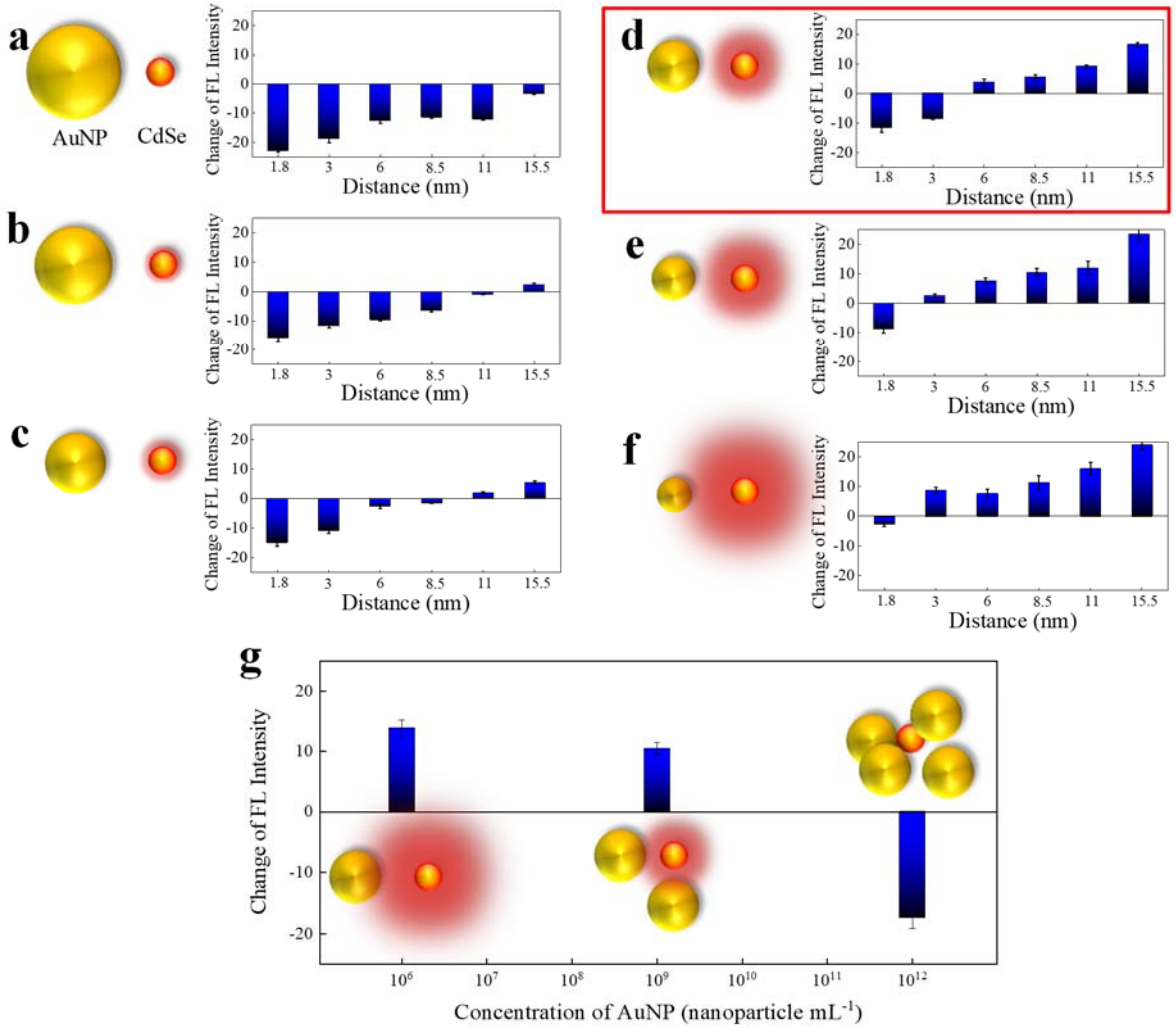

508

509

510 **Fig. 3.**

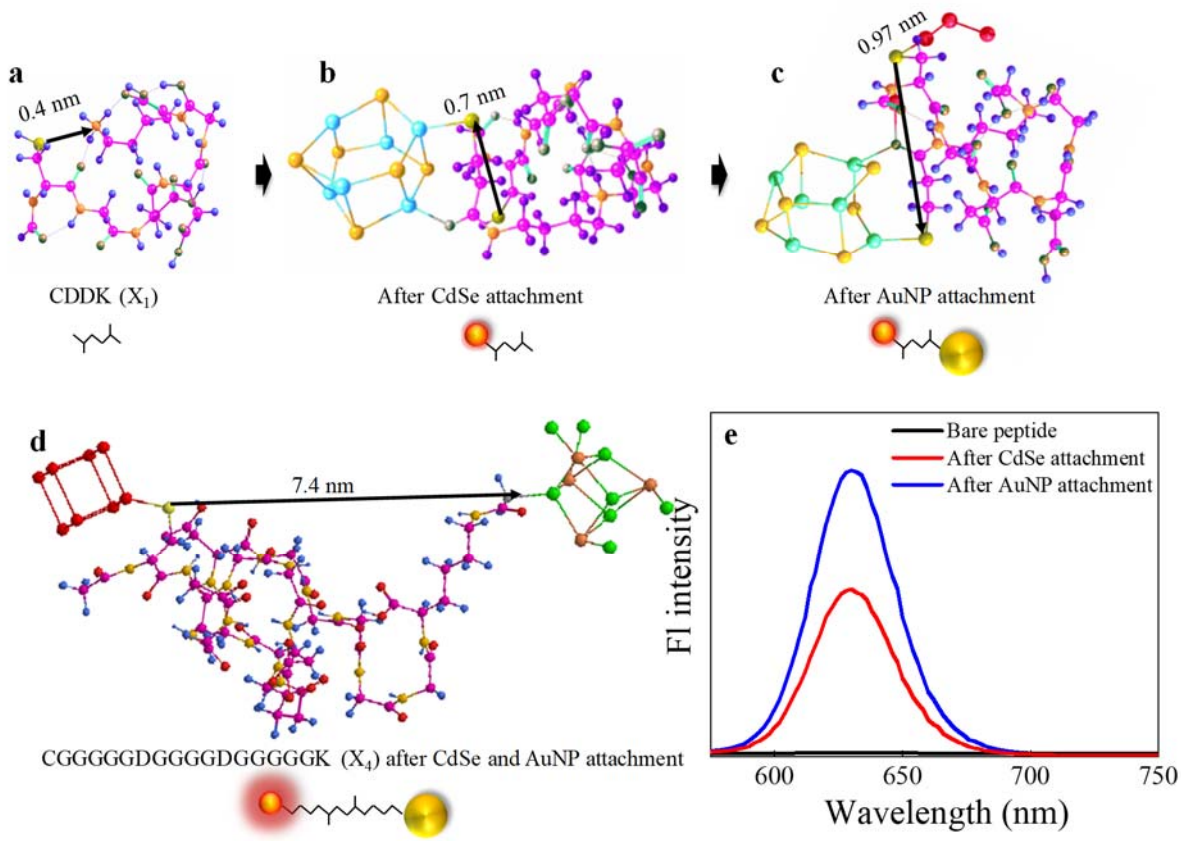

511

512

513 **Fig. 4.**

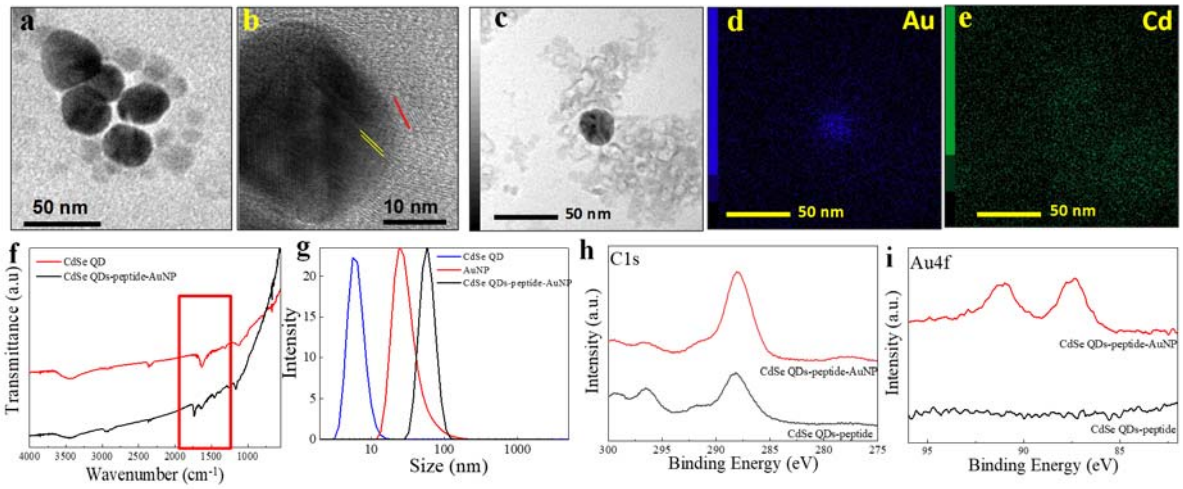

514

515

516 **Fig. 5.**

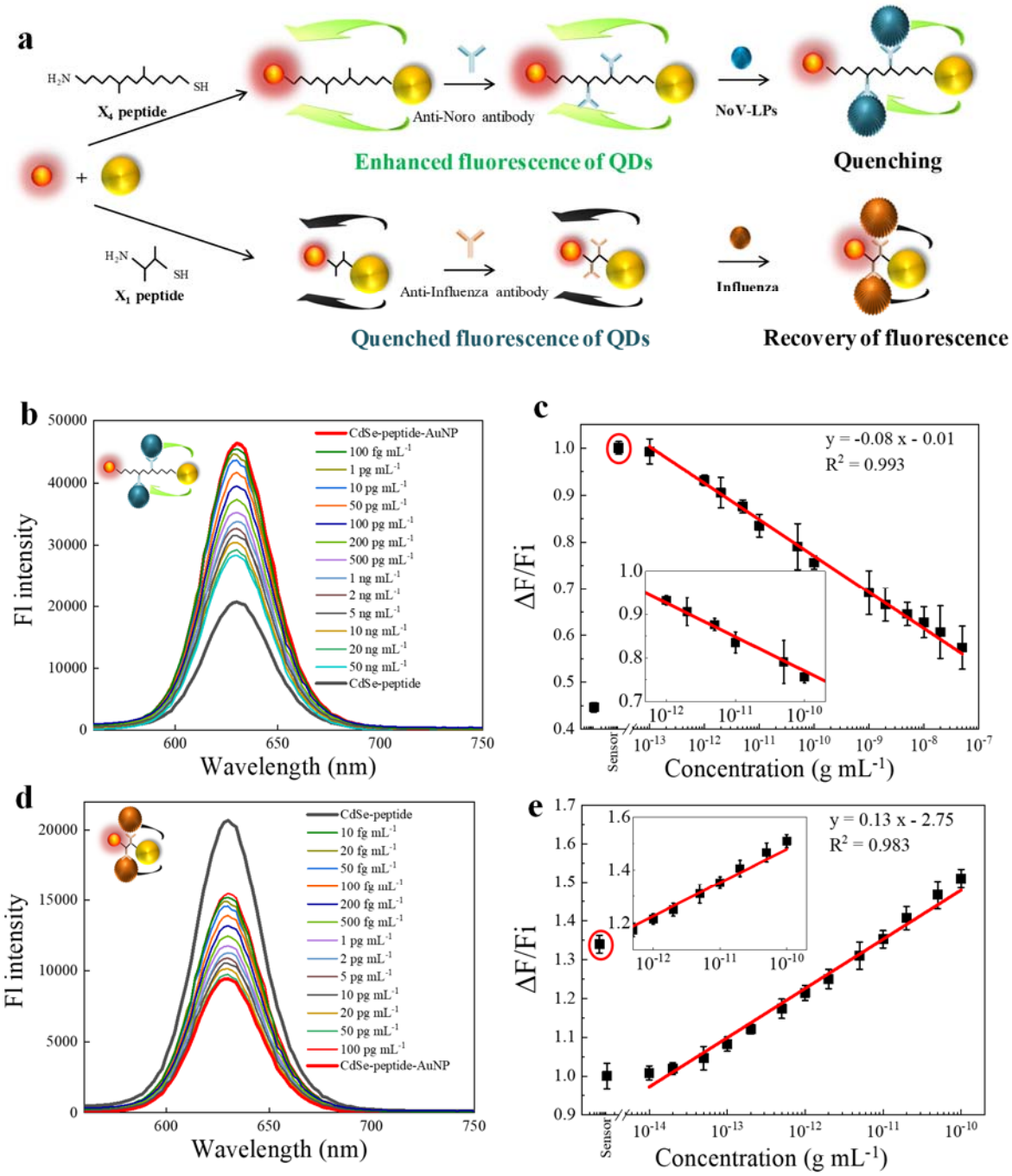

517

518

Supplementary Material

Controlling distance, size and concentration of nanoconjugates for optimized LSPR based biosensors

Ankan Dutta Chowdhury[a], Fahmida Nasrin[b], Rupali Gangopadhyay[c,#], Akhilesh Babu Ganganboina[a], Kenshin Takemura[b], Ikko Kozaki[d], Hiroyuki Honda[d], Toshimi Hara[e], Fuyuki Abe[e], Sungjo Park[f], Tetsuro Suzuki[g], Enoch Y. Park[a,b,*]

[a] *Research Institute of Green Science and Technology, Shizuoka University, 836 Ohya Suruga-ku, Shizuoka 422-8529, Japan*

[b] *Department of Bioscience, Graduate School of Science and Technology, Shizuoka University, 836 Ohya Suruga-ku, Shizuoka 422-8529, Japan*

[c] *University of Engineering and Management, Action Area III, New Town, Kolkata 100156, India*

[d] *Department of Biomolecular Engineering, Graduate School of Engineering, Nagoya University, Nagoya 464-8603, Japan*

[e] *Department of Microbiology, Shizuoka Institute of Environment and Hygiene, 4-27-2, Kita-13 ando, Aoi-ku, Shizuoka 420-8637, Japan*

[f] *Department of Cardiovascular Medicine, Mayo Clinic College of Medicine and Science, Mayo Clinic, 200 First Street SW, Rochester, MN, 55905, USA*

[g] *Department of Infectious Diseases, Hamamatsu University School of Medicine, 1-20-115 Higashi-ku, Handa-yama, Hamamatsu 431-3192, Japan*

---

[*]Corresponding author. Research Institute of Green Science and Technology, Shizuoka University, 836 Ohya Suruga-ku, Shizuoka 422-8529, Japan. E-mail: park.enoch@shizuoka.ac.jp

[#]Present Address: Sister Nivedita University, DG Block (Newtown), Action Area I, 1/2, Newtown, Kolkata 700156, India

E-mail: ankan.dutta.chowdhury@shizuoka.ac.jp (A.D. Chowdhury), fahmida.nasrin.17@shizuoka.ac.jp (F. Nasrin), camrg@iacs.res.in (R. Gangopadhyay), akhilesh.babu.ganganboina@shizuoka.ac.jp (A.B. Ganganboina), takemura.kenshin16@shizuoka.ac.jp (K. Takemura), kozaki.ikkou@b.mbox.nagoya-u.ac.jp (I. Kozaki), honda@chembio.nagoya-u.ac.jp (H. Honda), toshimi1_hara@pref.shizuoka.lg.jp (T. Hara), fuyuki1_abe@pref.shizuoka.lg.jp (F. Abe), park.sungjo@mayo.edu (SP), tesuzuki@hama-med.ac.jp (T. Suzuki), park.enoch@shizuoka.ac.jp (E.Y. Park)

Experimental Section

Chemicals: Chloroauric acid, N-(3-dimethylaminopropyl)-N-ethylcarbodiimide hydrochloride (EDC), N-hydroxysuccinimide (NHS), thioglycolic acid (TGA), cadmium oxide (CdO), hexadecylamine (HDA), trioctylphosphine oxide (TOPO), zinc oxide (ZnO), trioctylphosphine (TOP), 1-octadecene (ODE), sulfur (S) and selenium (Se) were purchased from Sigma Aldrich Co., LLC (Saint Louis, MO, USA). Sodium citrate, acetone, Tri-sodium citrate ($Na_3C_6H_5O_7$), potassium hydroxide, phosphate-buffered saline (PBS) and chloroform were bought from Wako Pure Chemical Ind. Ltd. (Osaka, Japan). Oleic acid (OA) was purchased from Nacalai Tesque Inc. (Kyoto, Japan). Norovirus-like particle (NoV-LP) preparation were followed by standard method (Ahmed et al. 2016; Jiang et al. 1992). Norovirus (NoV) was obtained from clinical feces samples collected from infected patients with infectious gastroenteritis, including foodborne illness, as determined by inspections based on laws and ordinances. The NoV concentration of these supernatants was evaluated to be: 7.2×10^8 RNA copy ml^{-1} by real-time-PCR. This NoV sampling was performed according to the guideline, after obtaining appropriate approvals from Ethics Committee of Environment and Hygiene Institute in Shizuoka Prefecture (September 14, 2016).

An anti-NoV antibody reactive to GII.4 (NS14 Ab) was prepared according to previous reports (Kitamoto et al. 2002; Kou et al. 2015). For the selectivity test, influenza virus A/H1N1 (New Caledonia/20/99) was purchased from Prospec-Tany Techno Gene Ltd. (Rehovot, Israel).

Fmoc photo-cleavable linker (sc-294977A, SANTA CRUZ, Texas, USA) was introduced at C-terminal end of peptides to allow to release peptides from the membrane. Then the membrane was irradiated with UV at 365 nm for 3 h using a transilluminator (DT-20LCP; Atto, Tokyo, Japan) to release a synthesized peptide, and punched using a biopsy punch (diameter,

6 mm; KAI Corp., Tokyo, Japan) to prepare a peptide-containing disk (peptide spot). Each disk was placed in a single well of a 96-well plate, 100 μL of 200 mM potassium phosphate buffer (pH 6.9) was added. Then the plate was centrifuged at 1000 rpm for 5 min to give a supernatant solution containing the soluble peptide.

Physicochemical Analysis: Surface morphology and size were confirmed by the images obtained from transmission electron microscopy (TEM) by using a TEM (JEM-2100F, JEOL, Ltd., Tokyo, Japan) at 100 kV. A hemispherical electron analyzer and an Al Kα X-ray source (1486.6 eV) was used to perform X-ray photoelectron spectroscopy (XPS, ESCA1600 system, ULVAC-PHI Inc.). Measurement of dynamic light scattering (DLS) was done by using a Zetasizer Nano series (Malvern Inst. Ltd., Malvern, UK). UV-Vis absorption and fluorescence emission were measured by using a filter-based microplate reader (Infinite F500, TECAN, Ltd, Männedorf, Switzerland). Energy dispersive spectroscopy (EDS) analysis was carried out by using a scanning electron microscopy system (JEM-16036, JEOL, Ltd., Tokyo, Japan) which is combined with JED-2300 EDS. Antibody conjugation to the QD-peptide-AuNP nanocomposites were confirmed by ELISA using a plate reader from Bio-Rad (Model 680; Hercules, USA). For characterizations of nanocomposites, Fourier transform infrared spectroscopy (FTIR) was recorded on FT/IR-6300 (JASCO, Japan) and Atomic force microscopy (AFM) in Nanoscope IV PicoForce Multimode atomic force microscope (Bruker, Santa Barbara, CA, USA) in contact mode.

Simulation of the interaction of CdSe QDs and AuNPs in CdSe QD-peptide-AuNP nanocomposites: In this work the interaction between peptides and two terminal nanoconjugates have been explored. For that purpose, energy minimized structures of three peptides were initially built up. After that they could interact with MPA-capped CdSe QD in one end and

AuNP in another end. The CdSe QD is supposed to be -SH functionalized after reaction with MPA and energy minimized structures of these molecules were also built up to understand the ultimate structure of the system.

All structures were built via Chemcraft, a structure building software, before modeling studies using density functional theory (DFT) as implemented in the Gaussian 03 suite of program. The structures of all molecules and complexes were determined by full geometry optimization in the gas-phase using B3LYP functional [02] with a moderate basis set that offers a reasonable trade-off between accuracy and computational resource. 3-21G**/6-31G**/LANL2DZ basis sets were employed for the present purpose. Frequency calculations were also performed to ascertain the stationary points. Only partial optimization was done for all Cd, Se, and Au atoms in the CdSe QD-peptide-AuNP nanocomposites (with optimized CdSe and AuNP) using 'modredundant' keyword. Both Au and $(CdSe)_6$ nanoclusters were arbitrarily chosen; the structural data of the $(CdSe)_n$ nanocluster was initially obtained from the Mercury database and was adjusted to $(CdSe)_6$ and optimized in the course of work. Although we have optimized the Au nanoclusters with a magic number of Au atoms (7, 13), $(CdSe)_8$, and $(CdSe)_{15}$, Au_4 and $(CdSe)_6$ clusters have been arbitrarily chosen for the initial two structure. The Au_8 has chosen for the last one due to the limitation of computational resources and to minimize computation time. Results of structural optimization of Au_4, $(CdSe)_6$-mercapto propanoic acid, and peptide chains with nanoclusters are discussed in the appropriate section.

Fluorometric detection of norovirus-like particles (NoV-LPs) or viruses using QD-peptide-AuNP sensing probe: Twenty µL of samples containing various concentrations of NoV-LPs was added in to the QD-peptide-AuNP sensing probe solution. After incubation for 3 min, the fluorescence intensity was measured. For the optimization, different sized of

nanocomposites with different chain length peptides were also performed in the same condition. The concentration range for the detection of NoV-LP was 10^{-14} – 10^{-9} g mL^{-1} which was performed in DI water. The wavelength for excitation of the sample solution was 450 nm and the emission wavelength for the measurement of fluorescence intensity was in a range of 500 – 700 nm. The same method was used for other viruses also.

X_6. AcO-CGGGGGGGGGGDGGGGGGGGGGDGGGGGGGGGGK (34) (~15.5 nm)

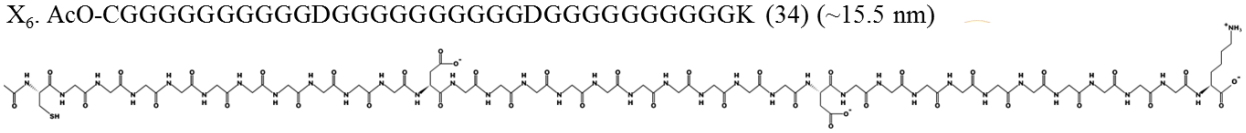

X_5. AcO-CGGGGGGGDGGGGGGDGGGGGGGK (24) (~11 nm)

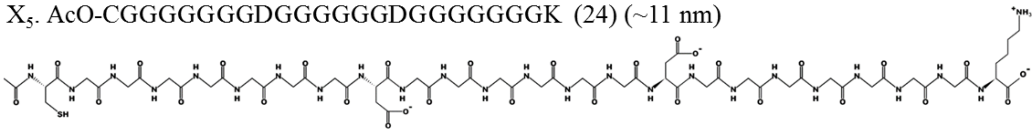

X_4. AcO-CGGGGGDGGGGDGGGGGK (18) (~8.5 nm)

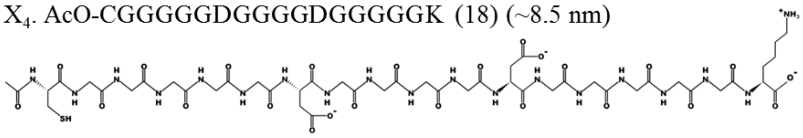

X_3. AcO-CGGGDGGDGGGK (12) (~6nm)

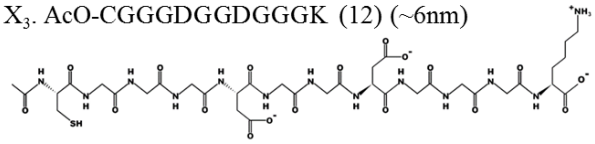

X_2. AcO-CGDDGK (6) (~3 nm)

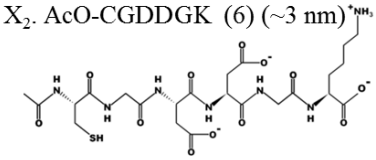

X_1. AcO-CDDK (4) (~1.8 nm)

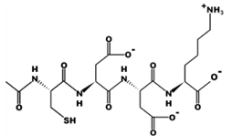

Fig. S1. All the peptide structures used for this study.

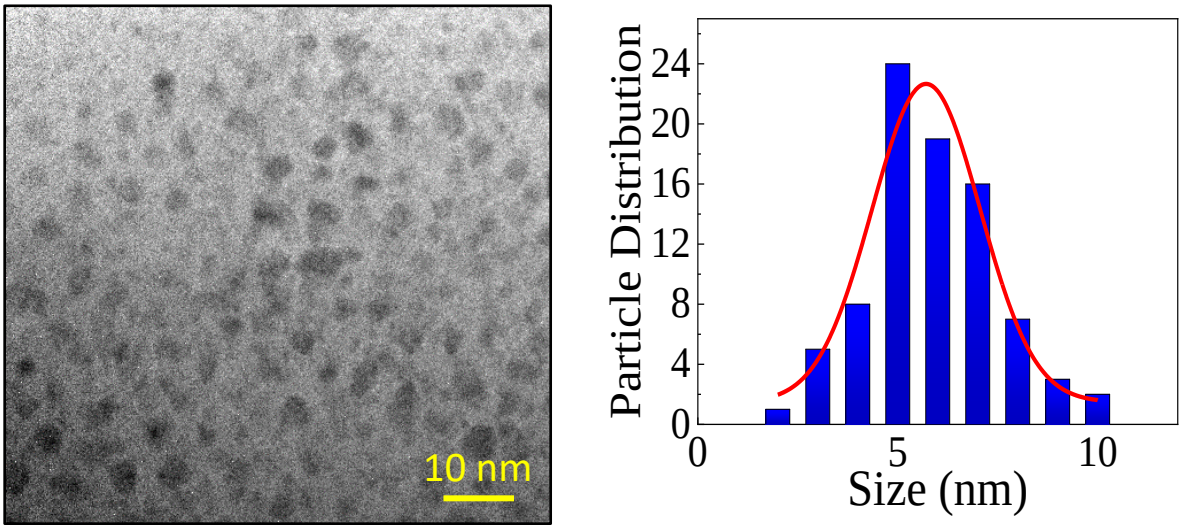

Fig. S2. Characterizations of CdSe QDs: TEM image of as synthesized CdSe QDs and its particle distribution.

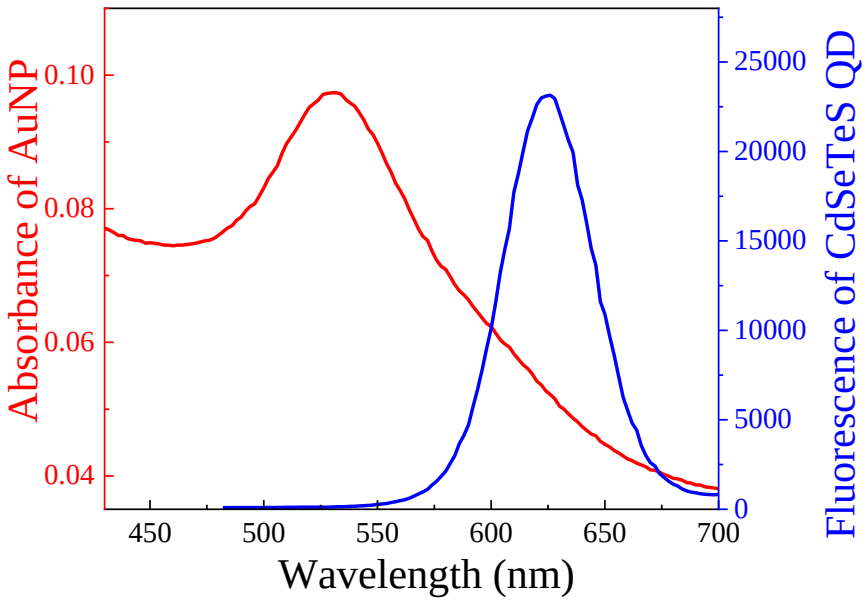

Fig. S3. Absorption and emission spectra of CdSe QDs.

Few optimized structures prior to optimization of the nanocomposite

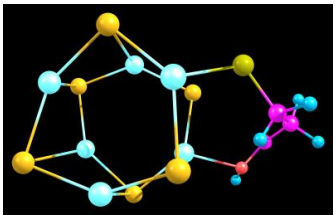

(a)

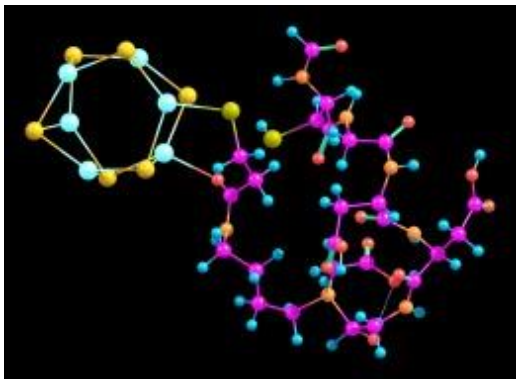

(b)

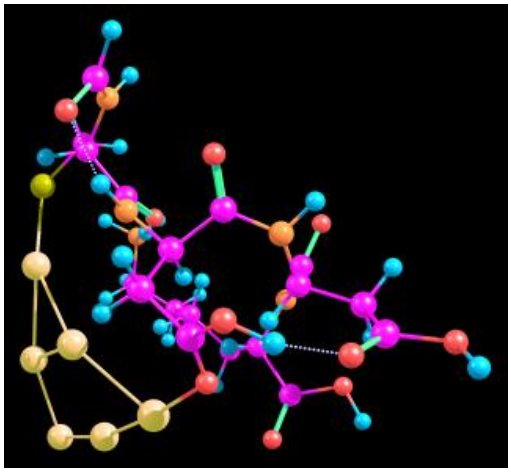

(c)

Fig. S4. Optimized structures of (a) $(CdSe)_6$ in combination with MPA, (b) Peptide in combination with Au_6-SH combination and (c) the peptide is linked with MPA coated CdSe QDs, which was optimized first before -attachment of AuNP.

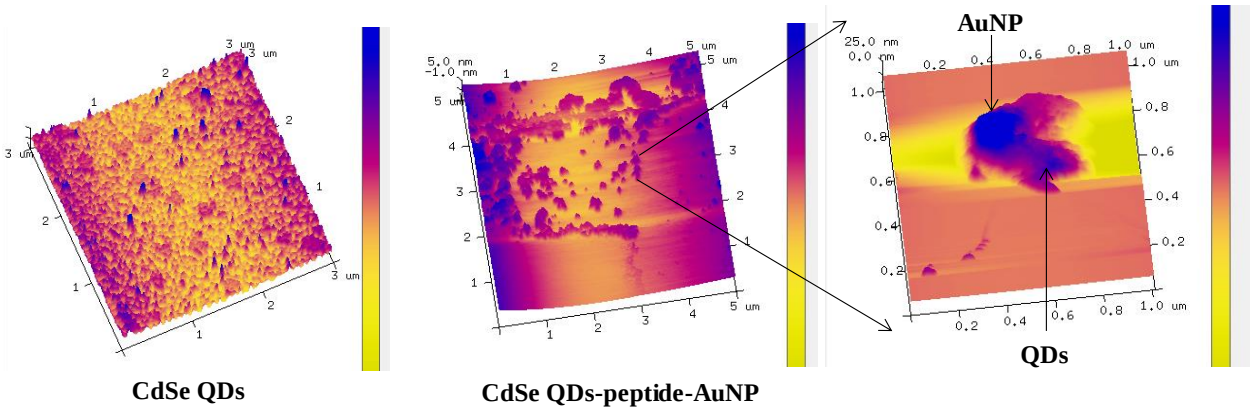

Fig. S5. AFM images of CdSe QDs and the CdSe QD-peptide X_4-AuNP nanoconjugate. The isolated picture of a single cluster of CdSe QD-peptide X_4-AuNP nanoconjugate indicate the binding of two nanoparticles by peptide linker.

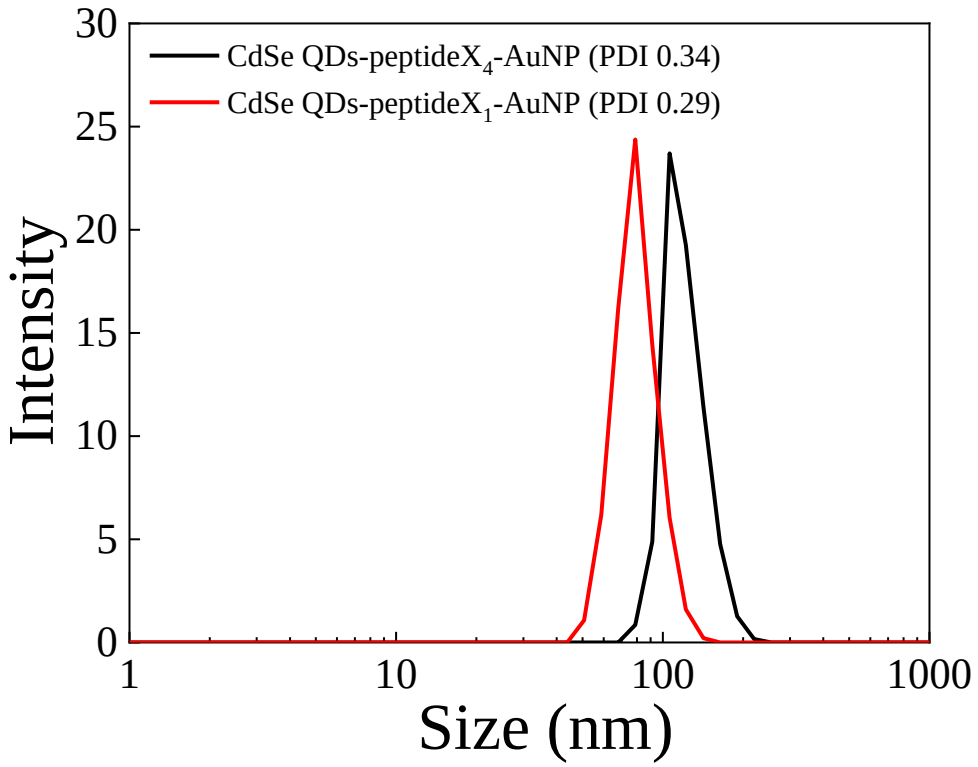

Fig. S6. Hydrodynamic sizes of CdSe QD-peptide-AuNPs with two extreme sizes of peptides.

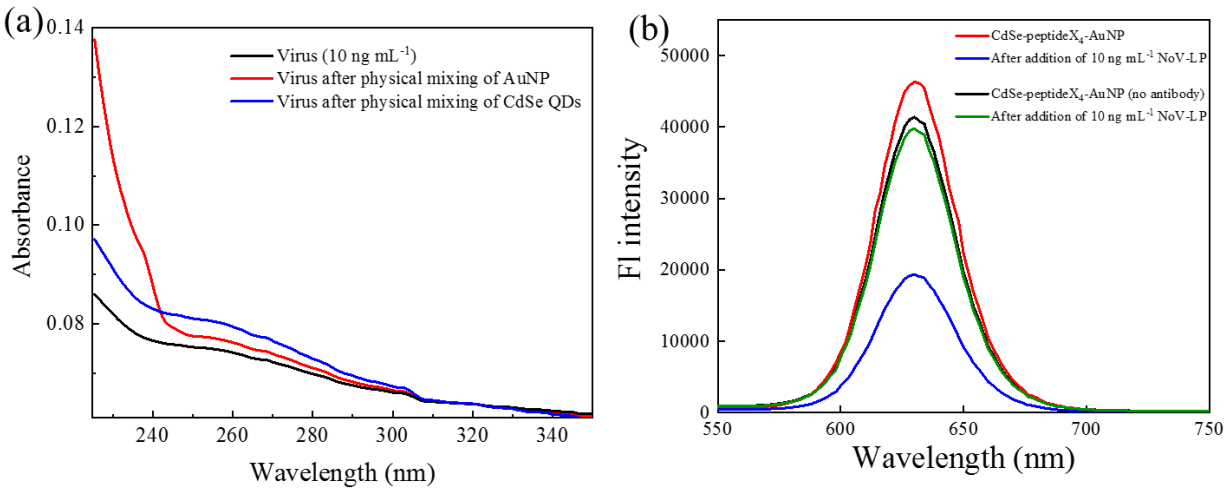

Fig. S7. (**a**) Absorbance of NoV-LP after physically mixed with CdSe QDs and AuNP individually, confirming the absence of nonspecific interaction, (**b**) fluorescence of CdSe QDs-peptideX_4-AuNP with viruses without antibody conjugation.

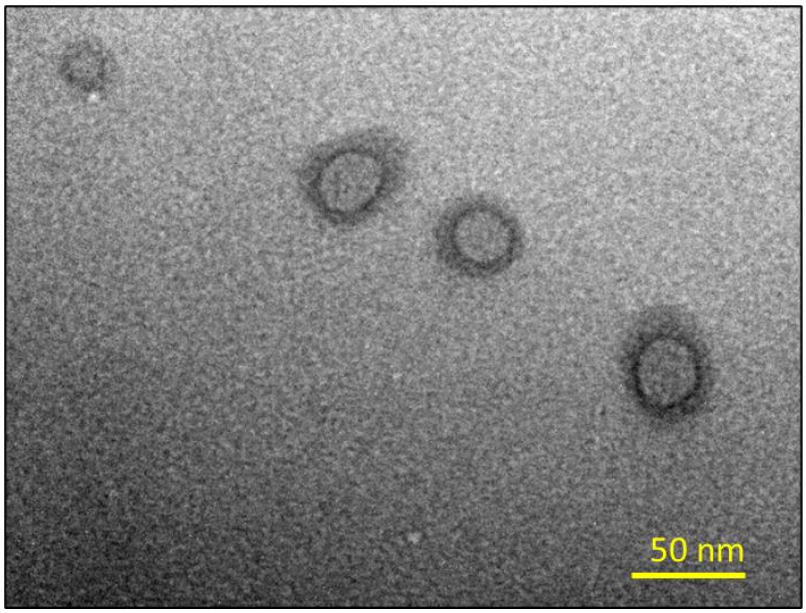

Fig. S8. TEM image of NoV-LP after PTA staining.

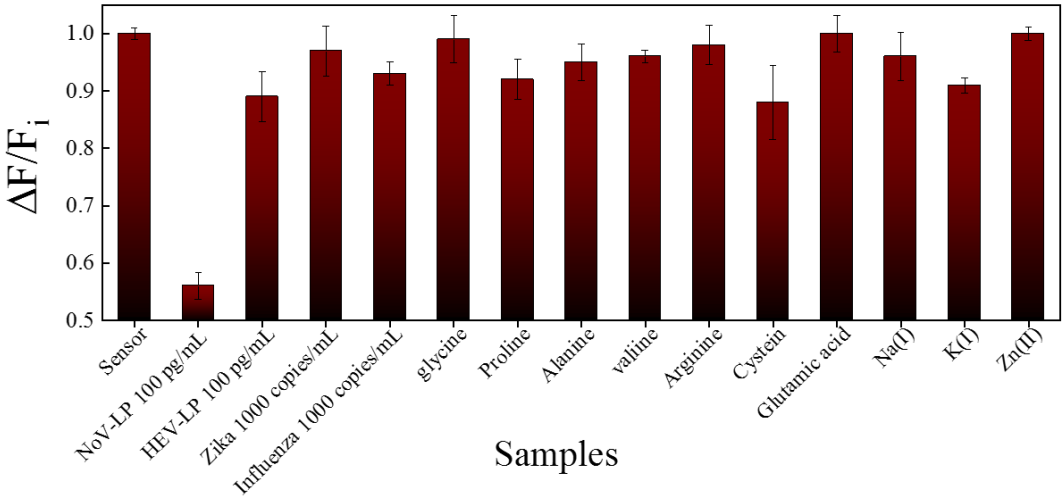

Fig. S9. Selectivity of the CdSe QD-peptide-AuNP biosensor: Used concentration of influenza virus, NoV-LP and HEV-LP were 100 pg mL^{-1}; Zika and influenza virus of 10^3 RNA copies mL^{-1}. Other common interfering was tested with metal ions (0.1 mg mL^{-1}) and amino acids (2 mM mL^{-1}).

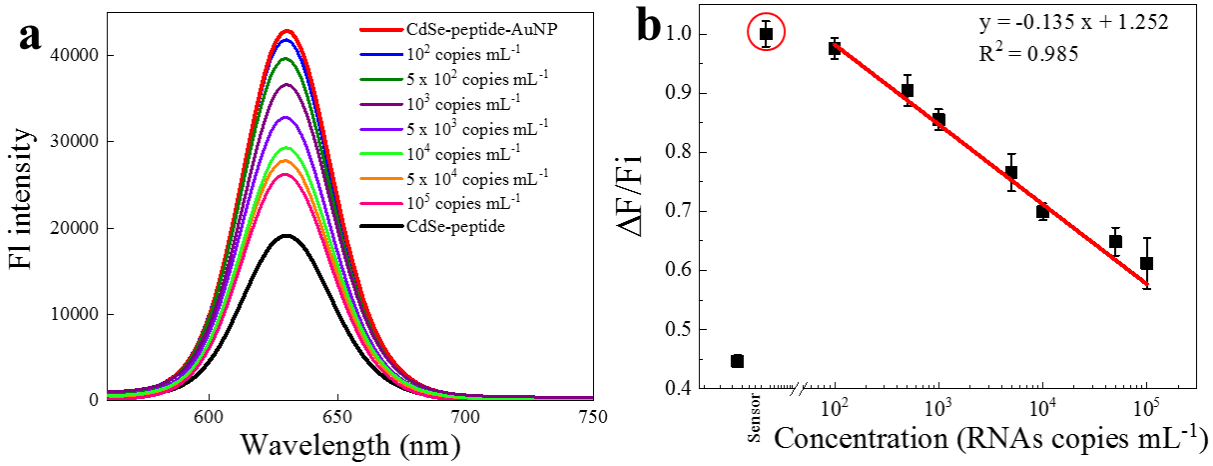

Fig. S10. (a) Fluorescence emission spectra for the detection of NoV in the concentration range of 10 – 10^5 RNA copies mL^{-1} and **(b)** its corresponding calibration curve. The red circle in the calibration graph indicates the blank sensor point. Error bars denote standard deviation of 3 replicate measurements.

References:

Ahmed, S.R., Kim, J., Suzuki, T., Lee, J., Park, E.Y., 2016. Biosen. Bioelectrons., 85, 503–508.

Jiang, X., Wang, M., Graham, D. Y., Estes, M. K., 1992. J. Virol., 66, 6527–6532.

Kitamoto, N., Tanaka, T., Natori, K., Takeda, N., Nakata, S., Jiang, X., Estes, M.K., 2002. J. Clin. Microbiol 40(7), 2459–2465.

Kou, B., Crawford, S.E., Ajami, N.J., Czakó, R., Neill, F.H., Tanaka, T.N., Kitamoto, N., Palzkill, T.G., Estes, M.K., Atmar, R.L., 2015. Clin. Vaccine Immunol. 22(2), 160–167.